Mechanical Systems and Signal Processing 124 (2019) 459–478

Contents lists available at ScienceDirect

Mechanical Systems and Signal Processing

journal homepage: www.elsevier.com/locate/ymssp

Matched-field processing for leak localization in a viscoelastic pipe: An experimental study

Xun Wang [a,*], Jingrong Lin [a,b], Alireza Keramat [a,c], Mohamed S. Ghidaoui [a], Silvia Meniconi [d], Bruno Brunone [d]

[a] Department of Civil and Environmental Engineering, Hong Kong University of Science and Technology, Clear Water Bay, Hong Kong, China
[b] Department of Earth, Ocean and Atmospheric Sciences, University of British Columbia, Vancouver, Canada
[c] Department of Civil Engineering, Jundi-Shapur University of Technology, Dezful, Iran
[d] Department of Civil and Environmental Engineering, University of Perugia, 06125 Perugia, Italy

ARTICLE INFO

Article history:
Received 1 August 2018
Received in revised form 17 December 2018
Accepted 2 February 2019
Available online 11 February 2019

Keywords:
Transient wave
Leakage localization
Matched-field processing
Pipe viscoelasticity
Complex environment

ABSTRACT

This paper applies the matched-field processing (MFP) method to leakage localization in a viscoelastic pipe. The viscoelasticity of pipe wall is included in the governing equations of transient wave via the generalized Kelvin-Voigt model and its effect is finally translated into a frequency-dependent wave speed. Then, a leak is localized by MFP via a 1D search of leak location along the pipe, independent of the leak size. Transient experiments with viscoelastic pipe in the Water Engineering Laboratory at University of Perugia and in the Water Resources Research Laboratory at Hong Kong University of Science and Technology are studied. Experimental results demonstrate that the inclusion of pipe wall viscoelasticity and using more frequencies (instead of using only resonant frequencies) improve significantly the leak localization accuracy. It is shown that the MFP leak localization is accurate even for a small leak (the flow ratio of leak and main pipe is approximately 10%) in a noisy environment: among 50 transient experiments, the maximum error of MFP leak localization is only 1.14 m and in the other 49 experiments the error is always lower than 1 m.

1. Introduction

Leakage in water supply systems results in financial losses from wastage of water and health risks since leaks are potential entry points for contaminants during low pressure intrusion events [1]. Since 1980s, fluid transient-based defect detection methodology has been used for leakage detection. It introduces hydraulic pressure waves, measures pressure response at specified location(s), and uses the information of reflection and damping due to leakages to estimate their locations in water pipe systems. Specific methodological examples of this approach are: (i) transient reflection-based method (TRM), such as [2–7]; (ii) transient damping-based method (TDM) by [8]; (iii) frequency response-based method (FRM) by [9–25]; and (iv) inverse transient analysis (ITA) method [26–29].

Real water supply pipeline system is often a highly noisy environment due to traffic, mechanical devices, turbulence, etc. While previous methods in the literature do not theoretically or analytically study the effect of noise using a probabilistic framework, a recent method, known as the matched-field processing (MFP) [21], estimate a leak based on the

* Corresponding author.
E-mail addresses: xunwang@ust.hk, xunwang00@gmail.com (X. Wang).

https://doi.org/10.1016/j.ymssp.2019.02.004
0888-3270/

Nomenclature

q	discharge oscillation
h	pressure head oscillation
x^L	leak location
z^L	pipe elevation at leak
s^L	leak size
Q_0^L, H_0^L	steady-state discharge and head of leak
Q_0	steady-state discharge of main pipe
x_m $(m = 1, \cdots, M)$	sensor coordinate
$\Delta\mathbf{h}$	head difference
$\mathbf{n}$	measurement noise
a_0	wave speed in elastic pipes
a_{ve}	wave speed in viscoelastic pipes
A	area of pipeline
l	pipe length
D	internal pipe diameter
ω	angular frequency
ω_{th}	fundamental frequency
M	sensor number
K	frequency number
FRF	frequency response function
FRM	frequency response-based method
HDPE	high-density polyethylene
ITA	inverse transient analysis
K-V	Kelvin-Voigt
MFP	matched-field processing
MFP-E	MFP based on the model of elastic pipe [21]
MFP-VE	MFP based on the model of viscoelastic pipe
TDM	transient damping-based method
TRM	transient reflection-based method

maximum signal-to-noise ratio (SNR) meaning that the MFP method provides precise localization estimates even in noisy environments. MFP is able to use all available frequencies, not just resonant frequencies, and does not need to identify which frequencies are resonant frequencies, such that the leak estimation is more robust. However, the MFP approach in [21] is based on a transient wave model in elastic pipes; its availability in viscoelastic pipes has not been studied.

Viscoelastic pipes, such as polyvinyl chloride (PVC), polyethylene (PE), and high-density polyethylene (HDPE), are ideally applicable in urban water supply systems due to their excellence resilience, low cost, and convenience in construction and maintenance. The viscoelastic effect of pipe deformation during transient pressure behavior has been investigated [30–37]. It is shown that the viscoelastic behavior changes the nature of transient wave. Leak detection methods that can deal with pipe viscoelasticity have been proposed [38,36]. However, these methods do not consider the effect of noise in their models and may thus not be applicable in a noisy environment.

In the present paper, the viscoelastic effect of pipe wall is included in the frequency-domain transient model, it is found that it can be equivalently quantified by changing the wave speed in the elastic case to be frequency-dependent. Then, MFP can be applied for leakage detection in a viscoelastic pipe; its efficiency is validated via experiments conducted in the Water Engineering Laboratory at University of Perugia and in the Water Resources Research Laboratory at Hong Kong University of Science and Technology. The accuracy of MFP in pipeline leakage localization and additional gain of using more frequencies, instead of only the resonant frequencies, which have been numerically justified via numerical simulation and theoretical analysis in [21,22], are experimentally illustrated in this paper. Experimental results show that the inclusion of pipe viscoelasticity in the transient model and in the leak detection scheme significantly increases the leak localization accuracy.

The organization of this paper is as follows. It begins with a description of transient wave model in a viscoelastic pipe system in Section 2. Section 3 introduces the MFP method for leak localization. The experimental setups, processing of data, and leakage localization results are introduced in Section 4. Based on the experimental results obtained in Section 4, Section 5 further discusses the issues of physical model, measurement information, and leak localization algorithm. Finally, conclusions are drawn in Section 6.

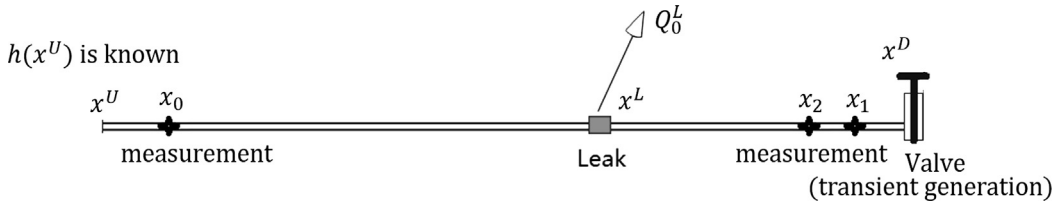

Fig. 1. Setup of the pipeline system.

2. Transient wave in a viscoelastic pipe

2.1. Governing equations in the time domain

The pipeline configuration is illustrated in Fig. 1. The upstream and downstream ends of the single pipe locate at $x = x^U = 0$ and $x = x^D = L$, respectively. The pressure head $h(x^U)$ at x^U is known and a transient generator is placed at x^D. A leak is assumed whose location is denoted by x^L, and z^L, Q_0^L and H_0^L denote the elevation of the pipe at the leak, the steady-state discharge and head at the leak, respectively. The lumped leak parameter $s^L = C^d A^L$ stands for the effective leak size, where C^d is the discharge coefficient of the leak and A^L is the flow area of the leak opening (orifice). The steady-state discharge of the leak is related to the lumped leak parameter by $Q_0^L = s^L\sqrt{2g\left(H_0^L - z^L\right)}$, in which g is the gravitational acceleration.

For a viscoelastic pipe, the total strain ϵ can be decomposed into an instantaneous-elastic strain ϵ_e and a retarded strain ϵ_r, i.e.,

$$\epsilon = \epsilon_e + \epsilon_r. \tag{1}$$

Let $\sigma(t)$ stand for dynamic stress at time t ($\sigma(t) = 0$ for $t \leqslant 0$), ϵ_e and ϵ_r read [39]:

$$\epsilon_e(t) = J_0\sigma(t), \tag{2}$$

$$\epsilon_r(t) = \int_0^t \sigma(t-s)\frac{dJ}{ds}ds, \tag{3}$$

in which $J_0 = J(0) = 1/E$ is the instantaneous creep-compliance representing the immediate response of the material, E is the Young's modulus of elasticity of pipe wall, and $J(t)$ is the creep function.

The discharge and pressure head oscillations due to a fluid transient are denoted by q and h. The linearized unsteady-oscillatory continuity and momentum equations with time t and spatial coordinate $x \in \left[x^U, x^L\right) \cup \left(x^L, x^D\right]$ [33,34] are

$$\frac{\partial q}{\partial x} + \frac{gA}{a_0^2}\frac{\partial h}{\partial t} + 2\left(1-\nu^2\right)A\frac{\partial \epsilon_r}{\partial t} = 0 \tag{4}$$

and

$$\frac{1}{gA}\frac{\partial q}{\partial t} + \frac{\partial h}{\partial x} + Rq = 0, \tag{5}$$

where unsteady friction is neglected and this is reasonable according to [35]. Here,

$$a_0 = \left(\rho\left(\frac{1}{\kappa} + \left(1-\nu^2\right)\frac{D}{Ee}\right)\right)^{-\frac{1}{2}} \tag{6}$$

is the elastic component of wave speed, κ and ρ are the bulk modulus and density of water, ν is the Poisson's ratio, D is the internal pipe diameter, and e is the pipe wall thickness. Furthermore, A is the area of pipeline, R is the steady-state resistance term being $R = (f_{DW}Q_0)/\left(gDA^2\right)$ for turbulent flows, f_{DW} is the Darcy-Weisbach friction factor, Q_0 is the steady-state discharge in the pipe. The last term of left hand side of Eq. (4) is due to pipe wall viscoelasticity; it equals to 0 in the elastic case since the creep function $J(t)$ is time-independent. Furthermore, ϵ_r here is the retarded circumferential strain and the influence of axial pipe velocity on Eqs. (4) and (5) is neglected.

Inserting Eq. (3) into Eq. (4) gives

$$\frac{\partial q}{\partial x} + \frac{gA}{a_0^2}\frac{\partial h}{\partial t} + 2\left(1-\nu^2\right)A\frac{\partial}{\partial t}\int_0^t \sigma(t-s)\frac{dJ}{ds}ds = 0. \tag{7}$$

Considering the force balance for the stress in the pipe wall and the pressure in fluid, i.e.,

$$2\sigma e = pD, \tag{8}$$

where $p = \rho g h$ is the dynamic pressure, we have

$$\sigma(t) = \frac{\rho g D}{2e} h(t). \tag{9}$$

Therefore, Eq. (7) becomes

$$\frac{\partial q}{\partial x} + \frac{gA}{a_0^2}\frac{\partial h}{\partial t} + (1-\nu^2)\frac{\rho g D A}{e}\frac{\partial}{\partial t}\int_0^t h(t-s)\frac{dJ}{ds}ds = 0. \tag{10}$$

2.2. Governing equations in the frequency domain and wave speed calibration for pipe wall viscoelasticity

Taking a Fourier transform of Eq. (10), it becomes

$$\frac{\partial q}{\partial x} + \frac{gA}{a_0^2}\mathrm{i}\omega h + (1-\nu^2)\frac{\rho g D A}{e}\mathscr{F}\left(\frac{\partial}{\partial t}\int_0^t h(t-s)\frac{dJ}{ds}ds\right) = 0, \tag{11}$$

where $\mathscr{F}(\cdot)$ stands for the operation of Fourier transform. The last term of Eq. (11) can be simplified by the Leibniz's rule for differentiation under the integral sign, the properties of Fourier transform and convolution, and $h(t) = 0$ for $t \leqslant 0$, as:

$$\begin{aligned} & \mathscr{F}\left(\tfrac{\partial}{\partial t}\int_0^t h(t-s)\tfrac{dJ}{ds}ds\right) \\ = \; & \mathscr{F}\left(h(0)\tfrac{dJ}{dt} + \int_0^t \tfrac{\partial h}{\partial t}(t-s)\tfrac{dJ}{ds}ds\right) = \mathscr{F}\left(\int_0^t \tfrac{\partial h}{\partial t}(t-s)\tfrac{dJ}{ds}ds\right) \\ = \; & \mathscr{F}\left(\tfrac{\partial h}{\partial t}\right)\mathscr{F}\left(\tfrac{dJ}{dt}\right) = \mathrm{i}\omega h\mathscr{F}\left(\tfrac{dJ}{dt}\right). \end{aligned} \tag{12}$$

Here, the creep function $J(t)$ is assumed to follow the generalized Kelvin-Voigt (K-V) model [31]:

$$J(t) = J_0 + \sum_{j=1}^{N_{kv}} J_j\left(1 - \exp(-t/\tau_j)\right), \tag{13}$$

where N_{kv} is the truncated order, J_j and τ_j are coefficients of the K-V model. Therefore, we have

$$\frac{dJ}{dt} = \sum_{j=1}^{N_{kv}} \frac{J_j}{\tau_j}\exp(-t/\tau_j) \tag{14}$$

and

$$\mathscr{F}\left(\frac{dJ}{dt}\right) = \sum_{j=1}^{N_{kv}} \frac{J_j}{1+\mathrm{i}\omega\tau_j}. \tag{15}$$

By Eqs. (12) and (15), Eq. (11) becomes

$$\frac{\partial q}{\partial x} + \frac{gA}{a_{ve}^2}\mathrm{i}\omega h = 0, \tag{16}$$

where

$$a_{ve} = \left(\rho\left(\frac{1}{\kappa} + (1-\nu^2)\frac{D}{e}\left(J_0 + \sum_{j=1}^{N_{kv}}\frac{J_j}{1+\mathrm{i}\omega\tau_j}\right)\right)\right)^{-\frac{1}{2}}. \tag{17}$$

Furthermore, taking Fourier transform of Eq. (5), we obtain

$$\frac{\partial h}{\partial x} + \left(\frac{\mathrm{i}\omega}{gA} + R\right)q = 0. \tag{18}$$

Eqs. (16) and (18) are respectively the continuity and momentum equations in the frequency domain. In the considered viscoelastic case where the pipe motion is assumed to be purely radial, the momentum equation Eq. (18) is same as the elastic case; the continuity equation changes but it is equivalent to replace the constant wave speed in the elastic case (a_0 in Eq. (6)) by the frequency-dependent a_{ve} in Eq. (17).

2.3. Boundary conditions and data model

Solving Eqs. (16) and (18) with boundary conditions of the discharge $q(x^U)$ and head $h(x^U)$ at x^U, for the case of $x_m < x^L$, the discharge and head (frequency response [40]) at a measurement station x_m can be computed as [41,42]:

$$\begin{pmatrix} q(x_m) \\ h(x_m) \end{pmatrix} = M^{NL}(x_m) \begin{pmatrix} q(x^U) \\ h(x^U) \end{pmatrix}, \tag{19}$$

in which

$$M^{NL}(x) = \begin{pmatrix} \cosh(\mu x) & -\frac{1}{Z}\sinh(\mu x) \\ -Z\sinh(\mu x) & \cosh(\mu x) \end{pmatrix} \tag{20}$$

is the field matrix,

$$Z(\omega) = \mu a_{ve}^2(\omega)/(\mathrm{i}\omega g A) \tag{21}$$

is the characteristic impedance,

$$\mu(\omega) = a_{ve}^{-1}(\omega)\sqrt{-\omega^2 + \mathrm{i}gA\omega R} \tag{22}$$

is the propagation function. In the case of $x_m > x^L$, by the head and mass conservation condition across the leak:

$$h(x^{L-}) = h(x^{L+}) = h(x^L); \tag{23}$$

$$q(x^{L-}) = q(x^{L+}) + q(x^L) = q(x^{L+}) + \frac{Q_0^L}{2\left(H_0^L - z^L\right)} h(x^L), \tag{24}$$

in which x^{L-} and x^{L+} represent respectively just upstream and downstream of x^L, the discharge and head at a measurement station x_m has the form [41,42]:

$$\begin{pmatrix} q(x_m) \\ h(x_m) \end{pmatrix} = M^{NL}(x_m - x^L) \begin{pmatrix} 1 & -\frac{Q_0^L}{2\left(H_0^L - z^L\right)} \\ 0 & 1 \end{pmatrix} M^{NL}(x^L) \begin{pmatrix} q(x^U) \\ h(x^U) \end{pmatrix}. \tag{25}$$

The transfer matrix on the right hand side of Eq. (25) can be further simplified as a form of variable separation of x^L and s^L [21,22]; the head at $x = x_m$ for a given angular frequency ω_k is [21]:

$$h(\omega_k, x_m) = h^{NL}(\omega_k, x_m) + s^L G(\omega_k, x^L, x_m), \tag{26}$$

wherein

$$h^{NL}(\omega_k, x_m) = -Z_k \sinh(\mu_k x_m) q(x^U, \omega_k) + \cosh(\mu_k x_m) h(x^U, \omega_k) \tag{27}$$

and

$$G(\omega_k, x^L, x_m) = \begin{cases} -\frac{\sqrt{g} Z_k \sinh\left(\mu_k\left(x_m - x^L\right)\right)}{\sqrt{2\left(H_0^L - z^L\right)}} \left(Z_k \sinh(\mu_k x^L) q(x^U, \omega_k) - \cosh(\mu_k x^L) h(x^U, \omega_k)\right), & x_m > x^L \\ 0, & x_m \leqslant x^L \end{cases}. \tag{28}$$

Assume that the measured heads at the frequency ω_k $(k = 1 \cdots, K)$ and at the location x_m $(m = 1 \cdots, M)$ are available and they are assumed to be contaminated by a noise n_{mk}, i.e.,

$$h(\omega_k, x_m) = h^{NL}(\omega_k, x_m) + s^L G(\omega_k, x^L, x_m) + n_{mk}. \tag{29}$$

By denoting

$$\Delta\mathbf{h} = (\Delta h_{11}, \cdots, \Delta h_{1K}, \cdots, \Delta h_{M1}, \cdots, \Delta h_{MK})^\top, \tag{30}$$

where

$$\Delta h_{mk} = h(\omega_k, x_m) - h^{NL}(\omega_k, x_m), \tag{31}$$

$$\mathbf{G}(x^L) = \left(G(\omega_1, x^L, x_1), \cdots, G(\omega_K, x^L, x_1), \cdots, G(\omega_1, x^L, x_M), \cdots, G(\omega_K, x^L, x_M)\right)^\top, \tag{32}$$

and

$$\mathbf{n} = (n_{11}, \cdots, n_{1K}, \cdots, n_{M1}, \cdots, n_{MK})^\top, \tag{33}$$

we finally have

$$\Delta\mathbf{h} = s^L\mathbf{G}(x^L) + \mathbf{n}. \tag{34}$$

In this paper, $\Delta\mathbf{h}$ is the data for leakage localization algorithm.

Note that in Eqs. (27) and (28), the boundary conditions at the upstream node $q(x^U)$ and $h(x^U)$ are assumed to be known. Here, $h(x^U)$ at the upstream boundary x^U is known, for example $h(x^U)$ can be reasonably assumed to be $h(x^U) = 0$ if the upstream is connected to a reservoir. The discharge $q(x^U)$ can be estimated if a transducer near the upstream boundary, whose location is denoted by x_0, is available [43,44]. Assuming there is no leak between x^U and x_0 and using the pressure head measurement $h(x_0)$ at x_0, the discharge $q(x^U)$ at the frequency ω_k can be estimated [22] by

$$\hat{q}(x^U, \omega_k) = \frac{\cosh(\mu_k(x_0 - x^U))h(x^U, \omega_k) - h(x_0, \omega_k)}{Z_k \sinh(\mu_k(x_0 - x^U))}. \tag{35}$$

3. Leak localization using the matched-field processing method

In this section, the leakage localization problem is solved using the MFP method. The noise vector $\mathbf{n}$ is assumed to follow a zero-mean Gaussian distribution $\mathcal{N}(\mathbf{0}, \sigma^2\mathbf{I}_{MK})$, where $\mathbf{I}_{MK}$ is a MK-dimensional identity matrix. Then, the leakage location can be estimated using MFP via [21]:

$$\widehat{x^L} = \arg\max_{x^L \in (0,l)} \frac{\Delta\mathbf{h}^H\mathbf{G}(x^L)\mathbf{G}^H(x^L)\Delta\mathbf{h}}{\mathbf{G}^H(x^L)\mathbf{G}(x^L)}. \tag{36}$$

Remark that the frequency-domain pressure is obtained from discrete Fourier transform, which is a linear combination of measured time-domain pressure signals, thus the frequency-domain noise can be approximately assumed as Gaussian distributed according to the Central Limit Theorem. A recent experimental investigation [45] also shows that, in a pipe with flow, the Gaussian assumption of noise distribution is reasonable. Furthermore, uncorrelated white noise (the covariance matrix is $\sigma^2\mathbf{I}_{MK}$) is assumed here; if the noise is non-white, a data transformation technique for noise whitening [21] can be applied before implementing MFP, such that the white noise assumption still holds and the leakage localization in Eq. (36) can still be used without changing its structure. This noise-whitening technique can improve the leak localization result when noise level is high according to the numerical results in [21].

Eq. (36) implies that a leak can be localized by a 1D search of leak location along the pipe, independent of its leak size. Physically, this is possible because the leak location determines the shape of FRF while the leak size only proportionally changes the magnitude of FRF at all the frequencies [15,46]. Essentially, MFP uses only the shape of FRF to localize leaks [21] such that the influence of leak size can be excluded.

Finally, the MFP algorithm of leakage localization in a viscoelastic pipe is summarized in Algorithm 1.

Algorithm 1 Localization of leakage in a viscoelastic pipe using MFP

1. Select K frequencies $\omega_1, \cdots, \omega_K$. The maximum frequency ω_K should not be higher than the maximum probing frequency. It is also suggested to use all available frequencies that are lower than the maximum probing frequency. The maximum probing frequency can be approximately computed from $1/T_c$ (T_c is the time duration of valve closure) or observed from the spectrum of measured signal.
2. Compute a_{ve} from Eq. (17) for each selected frequency ω_k ($k = 1, \cdots, K$), in which the viscoelastic coefficients N_{kv}, J_j and τ_j ($j = 1, \cdots, N_{kv}$) in the generalized K-V model are obtained prior to the transient test with leak.
3. Estimate the boundary condition $\hat{q}(x^U, \omega_k)$ for each selected frequency ω_k from Eq. (35) using the pressure head measurements from x_0.
4. Calculate $h^{NL}(\omega_k, x_m)$ via Eq. (27) and use the head differences $\Delta\mathbf{h}$ as the data, which includes pressure heads from K frequencies and M sensors ($x_1, \cdots, x_M$).
5. Plot the objective function in Eq. (36):

$$|B|^2 = \frac{\Delta\mathbf{h}^H\mathbf{G}(x^L)\mathbf{G}^H(x^L)\Delta\mathbf{h}}{\mathbf{G}^H(x^L)\mathbf{G}(x^L)} \tag{37}$$

with respect to x^L and retain x^L corresponding to maximum $|B|^2$ as leak location estimate.

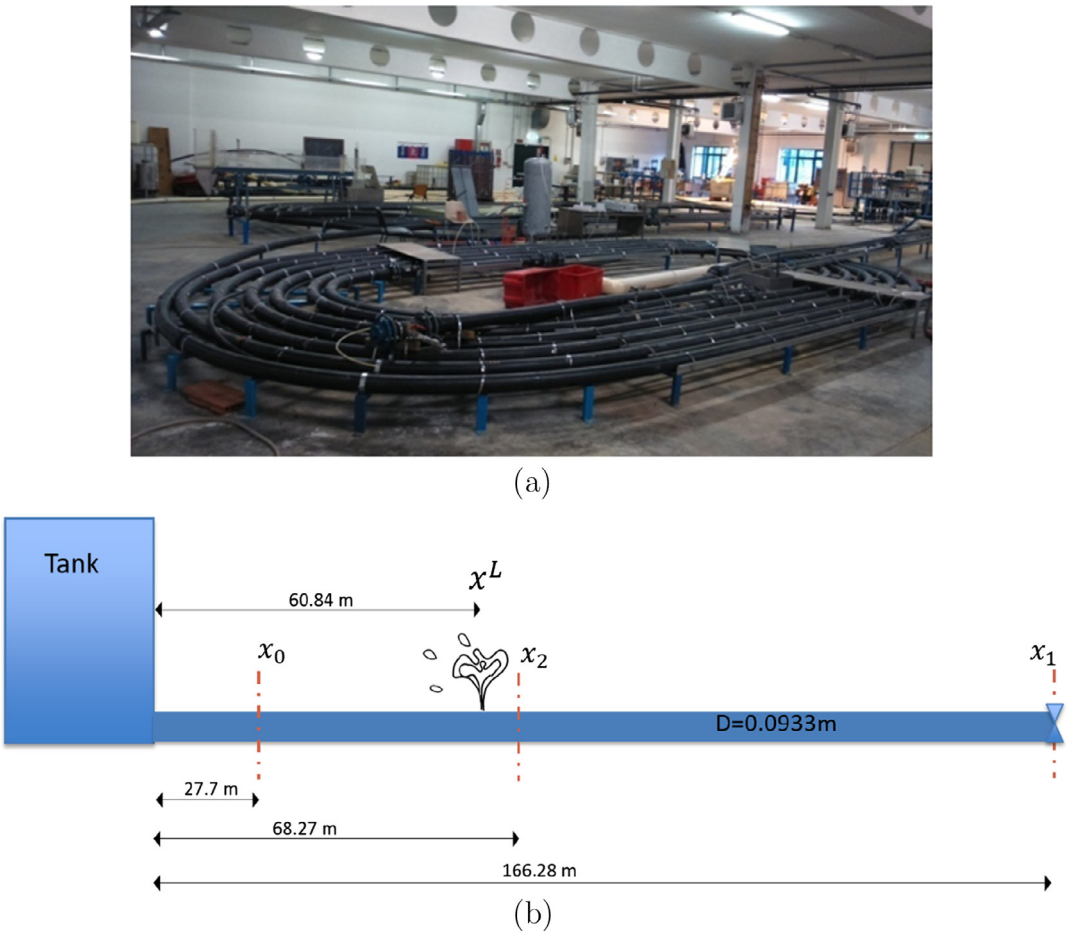

Fig. 2. (a) Photo and (b) sketch map of pipe transient experiment in the Water Engineering Laboratory at University of Perugia.

4. Experimental results

4.1. Experiments at University of Perugia

In this section, the MFP method for leak localization is tested using the water hammer experimental data obtained from the Water Engineering Laboratory of University of Perugia.

4.1.1. Experimental setup

The experimental setup is shown in Fig. 2. A HDPE pipe with length $l = 166.28$ m and internal diameter $D = 0.0933$ m is used. Transient wave is generated by a rapid and full closure of the downstream valve; the time duration of valve closure is approximately 0.1 s. Pressures are measured by three transducers located at $x_0 = 27.7$ m, $x_1 = 68.27$ m, and $x_2 = 166.28$ m, respectively. The average steady-state pressure head (pre-transient) at the upstream reservoir and at the valve are respectively 18.28 m and 17.09 m. The leak location is $x^L = 60.84$ m and the effective leak size is $s^L = 6.8 \times 10^{-5}$ m^2. By computing the travel time of the wave between the transducers, the wave speed is estimated as $a_0 = 375$ m/s. The Darcy-Weisbach friction factor is computed from the measured head loss as $f_{DW} = 0.0233$, according to the local velocity measurements carried out in [47].

4.1.2. Post-processing of measurements

The measured heads in time from the three sensors are shown in Fig. 3. Their system frequency response functions (FRFs) are obtained as follows.

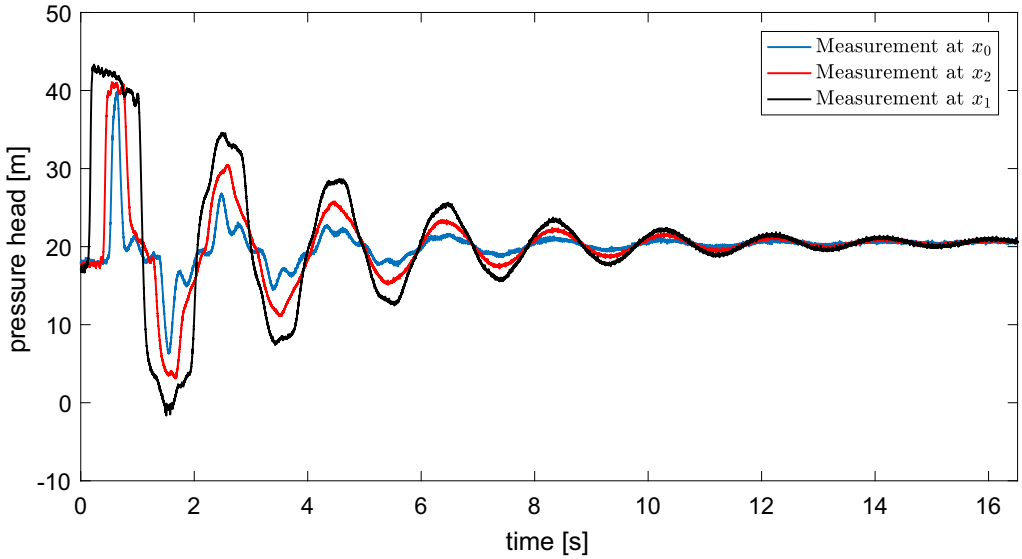

Fig. 3. Measured pressure in the time domain from the three transducers.

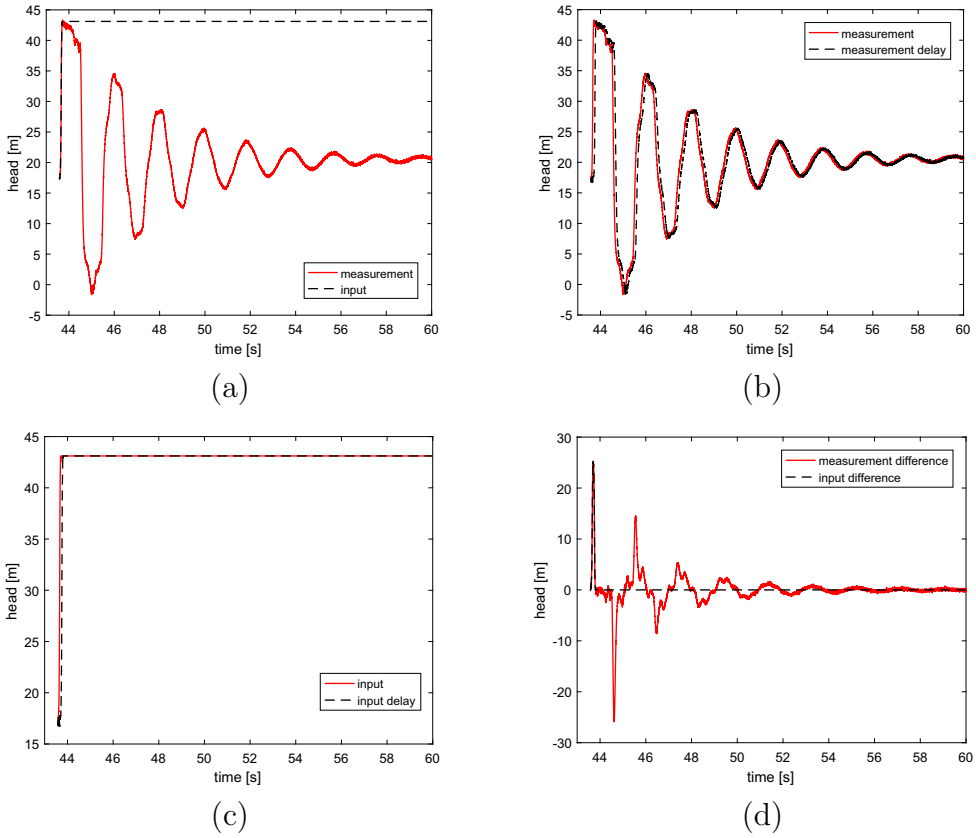

Fig. 4. Post-processing of measurement from the transducer at x_1: (a) the measurement and the computed input signal; (b) the measurement and its time delay; (c) the input signal and its time delay; (d) the difference of the measurement and its delay and the difference of the input signal and its delay.

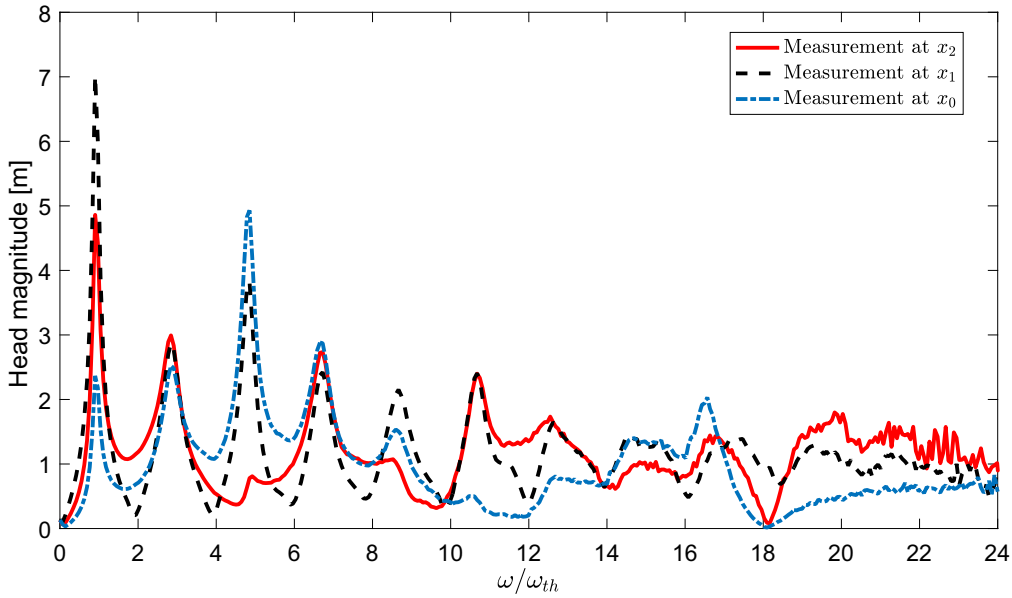

Fig. 5. Frequency response function of measurements from the three transducer.

Table 1
Coefficients for pipe wall viscoelasticity in the experiments at University of Perugia.

$\nu = 0.43$	$\kappa = 2.1 \times 10^9$ Pa	$\rho = 10^3$ kg/m^3
$D = 93.3 \times 10^{-3}$ m	$e = 7.5 \times 10^{-3}$ m	$J_0 = 0.68 \times 10^{-9}$ Pa^{-1}
$J_1 = 0.951 \times 10^{-10}$ Pa^{-1}	$\tau_1 = 0.05$ s	$J_2 = 1.065 \times 10^{-10}$ Pa^{-1}
$\tau_2 = 0.5$ s	$J_3 = 0.815 \times 10^{-10}$ Pa^{-1}	$\tau_3 = 1.5$ s

- Computing the FRF requires both the output from the system (the measured pressure head of transient wave in Fig. 3) and the input signal sent to the system. The latter is computed by selecting only the first step rise (from the last steady-state point to the maximum of the first jump) of the measurement and keeping it constant after the maximum point [48], since the input signal is generated by the full closure of valve. Fig. 4(a) takes the measurement from x_1 as an example which displays the measured head and the computed input signal.
- Note that these step time-series signals have infinite energy in theory (their integral from $-\infty$ to $+\infty$ equals to infinity), such that their spectra cannot be produced by a conventional Fourier transform [49]. Therefore, in order to change the signals into a finite energy form, each step signal is modified to a pulse-type signal by computing the difference between the original signal and its delay. The delay of the measurement or the input signal is computed by delaying the original signal with a time lag being longer than the time from the last steady-state point to the maximum of the first jump and being shorter than the time for the first reflection to arrive at the measure station [48]. The accuracy of this correction procedure does not depend on the time lag factor if it is in this range. Fig. 4(b) and (c) show the original signals and their delays of the measurement and the input, while Fig. 4(d) displays the differences (impulse-type signals) of the measured head and the input signal. According to the additive and distributive nature of time invariant linear systems, the frequency response of the system remains unchanged as a result of this operation (cf. Eq. (5.21) in [48]).
- Then, conventional Fourier transform is applied to the impulse-type output and input signals, which gives the corresponding frequency domain signals. Finally, the system FRF is obtained by their quotient. The FRFs versus ω/ω_{th} ($\omega_{th} = \pi a/(2l)$ is the fundamental frequency) at the three sensors are shown in Fig. 5.

4.1.3. Leak localization results

The calibrated frequency-dependent wave speed a_{ve} is obtained from Eq. (17), where the truncated order $N_{kv} = 3$ and the corresponding coefficients J_j and $\tau_j, j = 1, 2, 3$, are obtained (shown in Table 1) via a calibration of viscoelastic parameters of pipe material [50]. More specifically, a transient test without leak is done prior to the leaking test and the viscoelastic parameters are calibrated such that the transient wave model (without leak but J_j and τ_j are free parameters) is closest to the measured data. In fact, it is has been shown in [51,52] that the viscoelastic parameters obtained for a defect-free pipe allow simulating properly the transient behavior of a pipe with a defect.

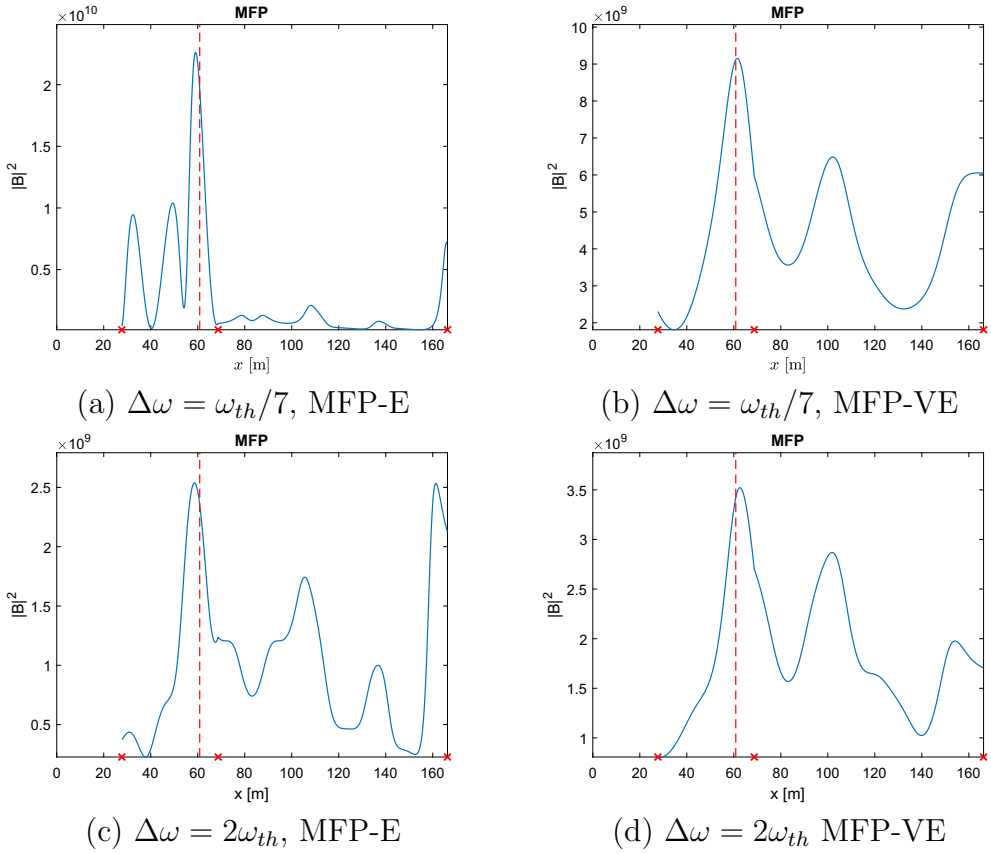

Fig. 6. Leak localization using MFP with different frequency spacing: (a,b) $\Delta\omega = \omega_{th}/7$ (i.e., in total 85 frequencies are used) and (c,d) $\Delta\omega = 2\omega_{th}$ (resonant frequencies only; in total 7 frequencies). In subfigures (a,c) and subfigures (b,d), the results are obtained with MFP-E and MFP-VE, respectively. The crosses and dash lines represent the sensor and actual leak locations, respectively.

In the following, the leak is localized using MFP. The leak detection results with and without the viscoelastic terms are both shown. To avoid confusion, we denote MFP-E as the MFP method based on the model of elastic pipe that does not include the viscoelastic terms (i.e., the method in [21]) and MFP-VE as the viscoelastic version of MFP proposed in the present paper. In MFP-E, the wave speed is $a_0 = 375$ m/s.

The upstream discharge $q(x^U)$, which appears in both h^{NL} and G in Eq. (34), is estimated via Eq. (35), in which $h(x_0)$ is the frequency response from the upstream transducer $x_0 = 27.7$ m. The choice of frequencies is an important issue for MFP. First, the maximum frequency included in the data $\Delta\mathbf{h}$ (or bandwidth) should be decided. In Fig. 5, the shape of FRF can be clearly seen for low frequencies, but the signal of transient wave becomes weak as the frequency increases. As a matter of fact, it can be observed from Fig. 5 that the data of FRF are not reliable when $\omega/\omega_{th} > 15$ in this experiment and is mainly comprised of noise. Second, the number of used frequency (in the given frequency range) also affects the localization results. It has been shown in [21] that with a given bandwidth using more frequencies increases the robustness of leak localization, particularly in a noisy environment.

Fig. 6 shows the leak localization results using MFP. Here, the used angular frequencies are denoted by $\{\omega : \omega_{th}, \omega_{th} + \Delta\omega, \omega_{th} + 2\Delta\omega, \cdots, n\omega_{th}\}$. Fig. 6(a) and (b) displays the results for $n = 13$ (i.e., seven peaks the in FRFs) and $\Delta\omega = \omega_{th}/7$ (i.e., in total 85 frequencies are used) using MFP-E and MFP-VE, respectively. It is clear that the model without viscoelasticity leads to a bias of leak localization (the error is 1.74 m) and the model with viscoelasticity improves the precision (the error is 0.66 m). This illustrates the importance of including viscoelasticity in the detection scheme. Fig. 6(c) and (d) shows the corresponding results with resonant frequencies only. In the case without including pipe viscoelasticity, a higher peak of MFP objective function appears near the downstream end of the pipe which results in a wrong estimate of leak location. The result is better when the viscoelasticity is considered but the error (1.76 m) is still larger than using more frequencies (0.66 m in Fig. 6(b)).

The localization error with different frequency bandwidth ($n = 5, 7, \cdots, 17$) and frequency step size ($\Delta\omega = \omega_{th}/7, \omega_{th}/2, \omega_{th}, 2\omega_{th}$) are shown in Fig. 7. These results clearly show that MFP-VE improves the leak localization accuracy. Furthermore, this figure justifies that using more frequencies in a given range decreases the localization error.

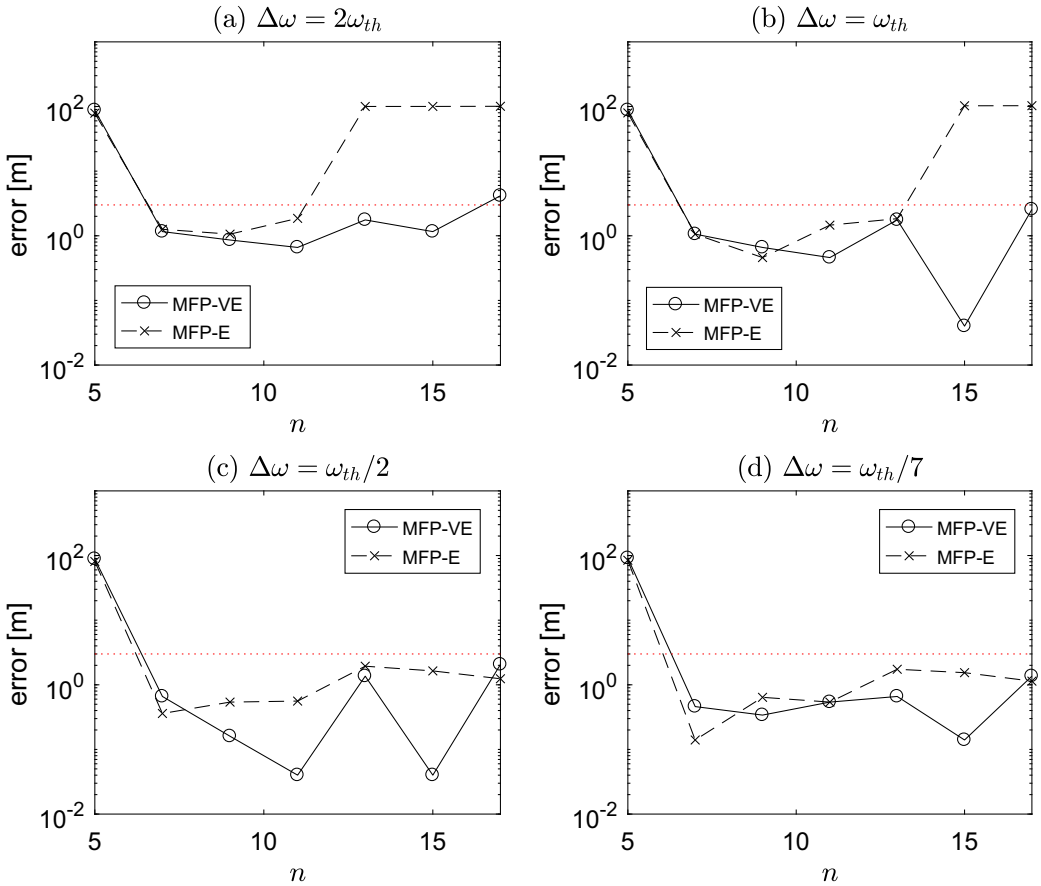

Fig. 7. Leak localization error with different frequency spacing (a) $\Delta\omega = 2\omega_{th}$ (resonant frequencies only); (b) $\Delta\omega = \omega_{th}$ (resonant and anti-resonant frequencies); (c) $\Delta\omega = \omega_{th}/2$; and (d) $\Delta\omega = \omega_{th}/7$. The solid and dash lines respectively stand for MFP-E and MFP-VE.

Table 2
The chosen maximum frequency such that the leak localization error less than 5 m (represented by n in the second column) and the average error of leak localization in the corresponding frequency range with various frequency spacing $\Delta\omega = 2\omega_{th}, \omega_{th}, \omega_{th}/2, \omega_{th}/7$.

$\Delta\omega$	n	Average error [m]	
		MFP-E	MFP-VE
$2\omega_{th}$	7 – 11	1.39	0.89
ω_{th}	7 – 13	1.21	0.99
$\omega_{th}/2$	7 – 17	1.04	0.72
$\omega_{th}/7$	7 – 17	0.96	0.58

In the cases where $\Delta\omega = \omega_{th}/7, \omega_{th}/2$, the error is always less than 5 m (labeled by the dotted lines in Fig. 7) for all the frequency ranges except $n = 5$ where too little information is available. By contrast, only using resonant frequencies (or even with anti-resonant frequencies together) obviously increases the error; including viscoelasticity becomes more important and the choice of frequency range must be careful. The working frequency (here, "working" means the localization error is less than 5 m) for the four cases of $\Delta\omega$ is listed in the second column of Table 2. This table also displays the average error for each $\Delta\omega$ in the corresponding working range of frequency, which illustrates again the importance of including viscoelasticity in the leak detection scheme and using more frequencies.

4.2. Experiments at Hong Kong University of Science and Technology

This section applies the MFP leak localization method to the experimental results obtained from the newly-built water pipe system at the Water Resources Research Laboratory at Hong Kong University of Science and Technology.

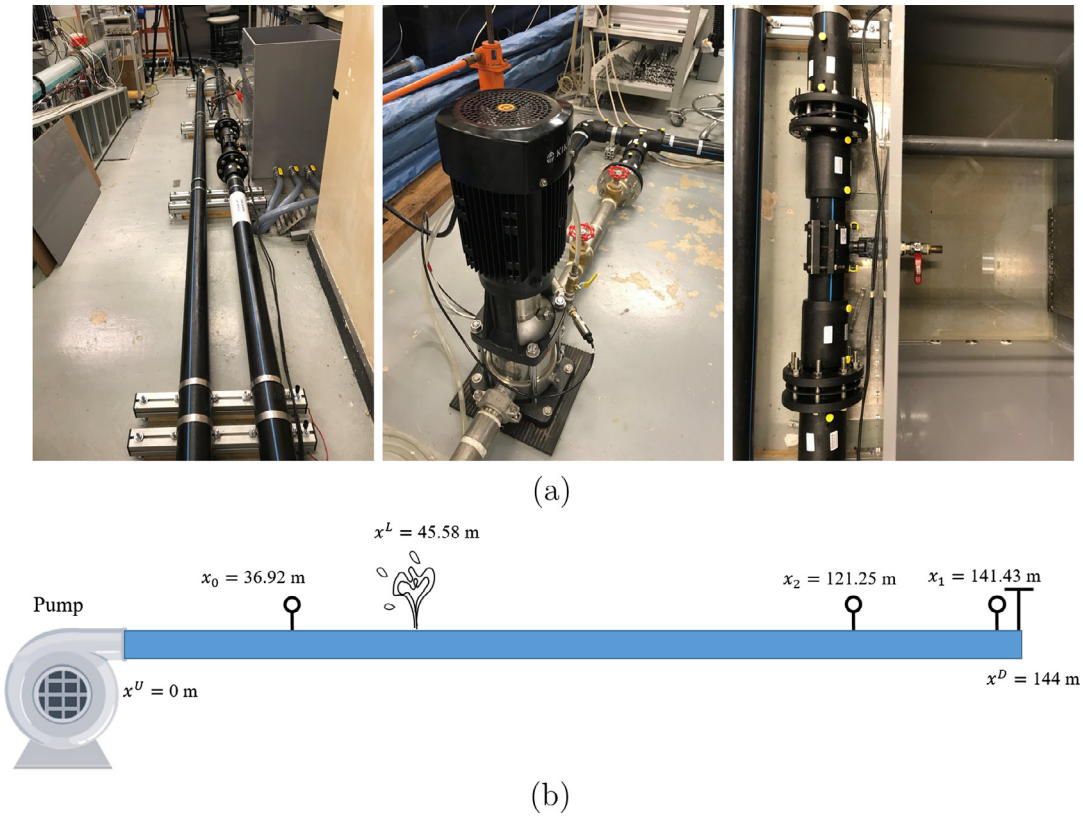

Fig. 8. (a) Photos (pipe (left), pump (middle), and leak (right)) and (b) sketch map of pipe transient experiment in the Water Resources Research Laboratory at Hong Kong University of Science and Technology.

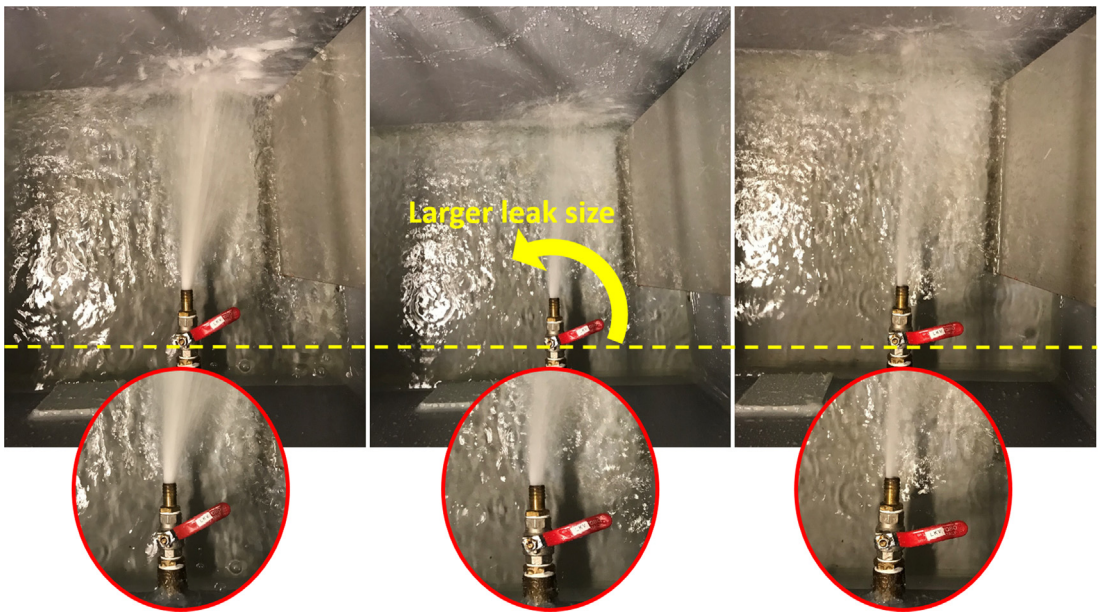

Fig. 9. Photos of three different leak sizes in the experiments at Hong Kong University of Science and Technology. The flow rate ratio between the main and the leak is 40% (left), 20% (middle), and 10% (right), respectively.

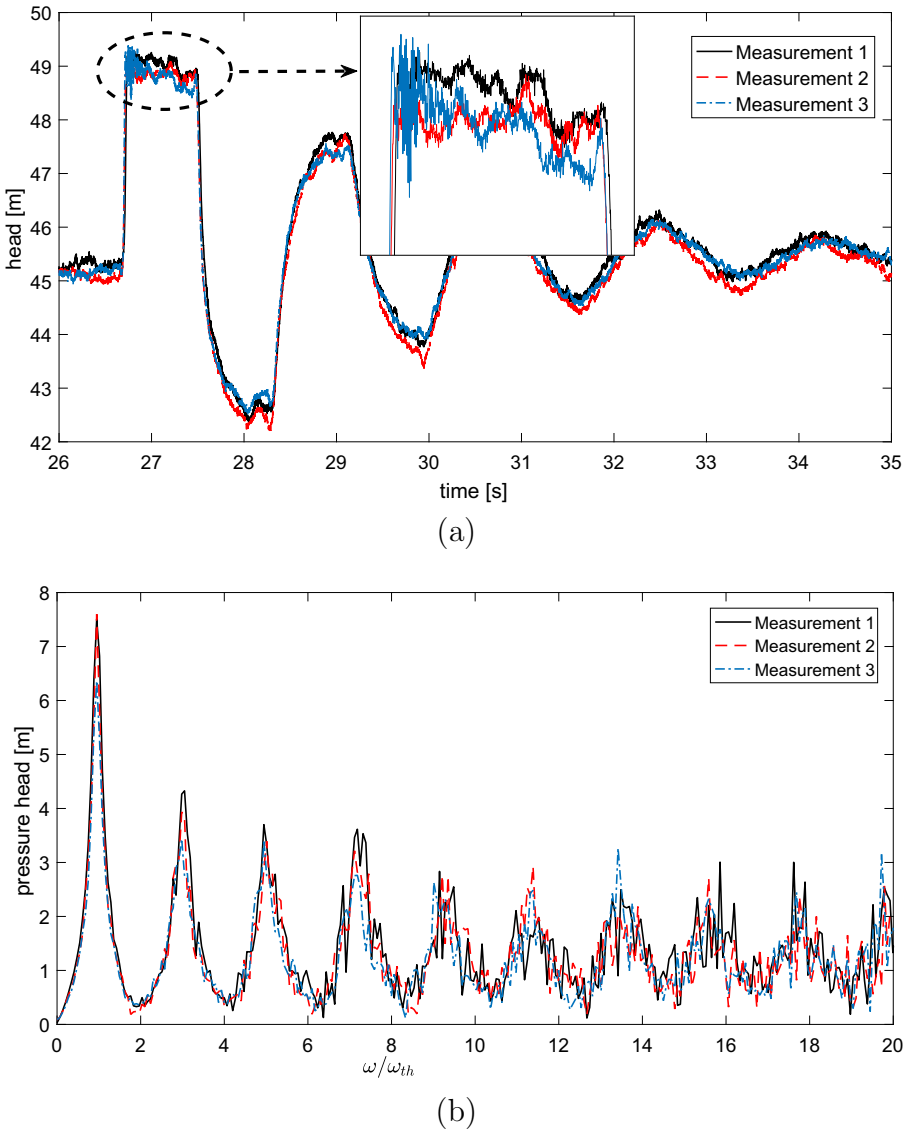

Fig. 10. Three different measurements obtained from the sensor $x_1 = 141.43$ m in the time domain (a) and in the frequency domain (b).

4.2.1. Experimental setup and measurements

The setup of HDPE pipeline system is shown in Fig. 8. The pipe length is $l = 144$ m and the internal diameter is $D = 0.0792$ m. A pump (in Fig. 8(a) middle), instead of the surge tank used in the experiments conducted at University of Perugia, is connected to the upstream of pipe. A downstream valve is used to generate transient waves; the time closure is approximately 0.05 s. Three hydrophones at $x_0 = 36.92$ m, $x_1 = 141.43$ m and $x_2 = 122.25$ m are set in the pipe to measure pressure. A leak locates at $x^L = 45.58$ m (in Fig. 8(a) right); the leak size can be changed via different valve settings. Three different leak sizes are tested, as shown in Fig. 9, because leak size is crucial in terms of leak detectability [53]. The three tests correspond to the following steady-state flow ratio of leak and main pipe: $Q_0^L/Q_0 = 40\%, 20\%, 10\%$. The leak flow Q_0^L and the pipe flow Q_0 are measured from two flow meters just upstream and just downstream of the leak.

Fig. 10(a) shows three different measured pressure head signals (i.e., from three different water hammer experiments) at $x_1 = 141.43$ m, where $Q_0^L/Q_0 = 40\%$. It can be seen from this figure that the measured signals are much more noisy and aleatory, and have more uncertainties than those in Fig. 3 (experiments at University of Perugia). A similar phenomenon can be observed by the corresponding FRFs in Fig. 10(b), which are also much more noisy than those in Fig. 5. This may be partially due to the pump, which itself generates much noise. The presence of the noise and uncertainty makes the leak localization more challenging:

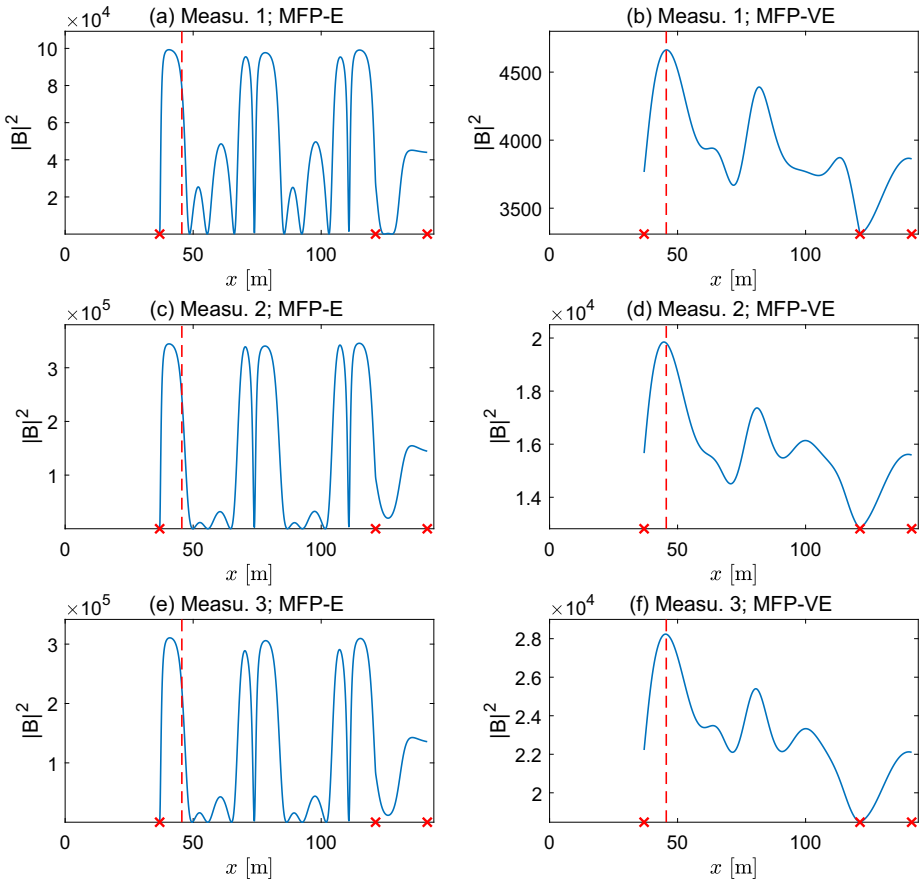

Fig. 11. Leak localization using MFP-E (a,c,e) and MFP-VE (b,d,f). The three measurements shown in Fig. 10 are respectively used.

Table 3
Coefficients for pipe wall viscoelasticity in the experiments at Hong Kong University of Science and Technology.

$\nu = 0.43$	$\kappa = 2.1 \times 10^9$ Pa	$\rho = 10^3$ kg/m^3
$D = 79.2 \times 10^{-3}$ m	$e = 5.4 \times 10^{-3}$ m	$J_0 = 4.8 \times 10^{-10}$ Pa^{-1}
$J_1 = 1.957 \times 10^{-10}$ Pa^{-1}	$\tau_1 = 0.038$ s	$J_2 = 1.0954 \times 10^{-10}$ Pa^{-1}
$\tau_2 = 0.6$ s	$J_3 = 9.05 \times 10^{-12}$ Pa^{-1}	$\tau_3 = 1.5$ s

- In Measurement 2 in Fig. 10(a), the pressure drop due to leak is not obvious even if the leak is large ($Q_0^L/Q_0 = 40\%$). This unclear reflection due to leak may mean that some reflection-based leak detection methods fail.
- In Measurement 3 in Fig. 10(a), a very strong noise can be seen in the first period of time signal, which may disturb some signal processing techniques.
- The FRFs in Fig. 10(b) are noisy and the resonant frequencies are not so clear as in the experiments at University of Perugia (cf. Fig. 5). This poses a challenge for methods based on resonant frequencies.

Moreover, the MFP method needs $\hat{q}(x^U)$ which is estimated via Eq. (35). Here, it is assumed $h(x^U) = 0$ in the computation of Eq. (35). However, unlike the experiments in Section 4.1 where a reservoir is connected to the pipe upstream to keep the pressure head constant, in the experiments in this section a pump is used such that the assumption $h(x^U) = 0$ could result in uncertainties in the model.

4.2.2. Leak localization results

Fig. 11 shows the MFP leak localization results using the three measurements in Fig. 10. Here, the frequencies used are all available frequencies from ω_{th} to $17\omega_{th}$. The MFP without viscoelastic calibration (MFP-E) results in bad results; in

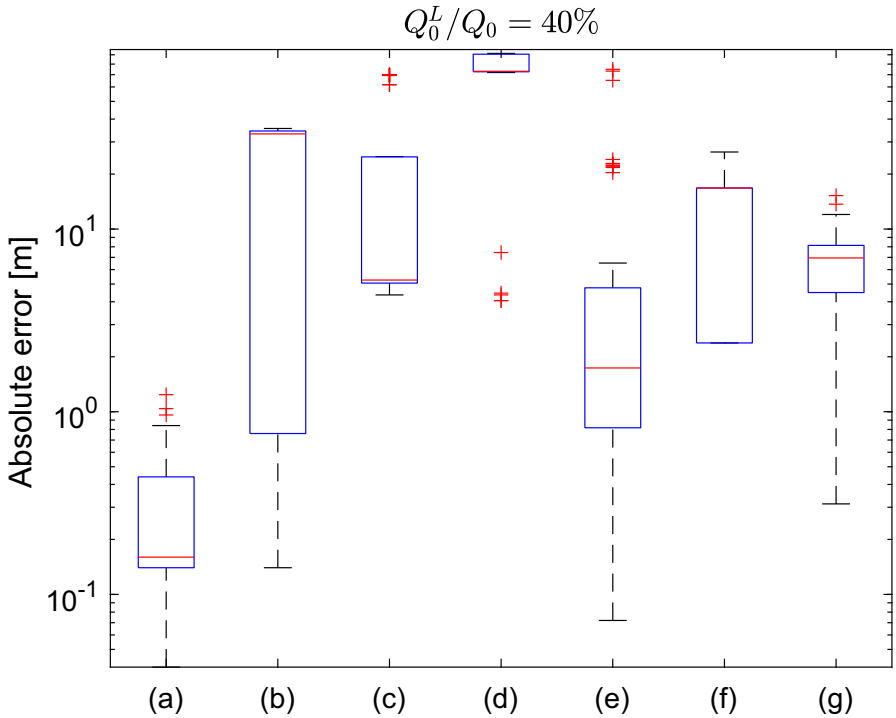

Fig. 12. Box plot of absolute error of leak localization obtained from 50 water hammer experiments. The methods used for leak localization is (a) MFP-VE with all frequencies; (b) MFP-VE with only resonant frequencies; (c) MFP-E with all frequencies; (d) MFP-E with only resonant frequencies; (e) wavelet transform method; (f) FRF peak pattern method; (g) ITA method. The ratio Q_0^L/Q_0 of leak flow and main flow is 40%.

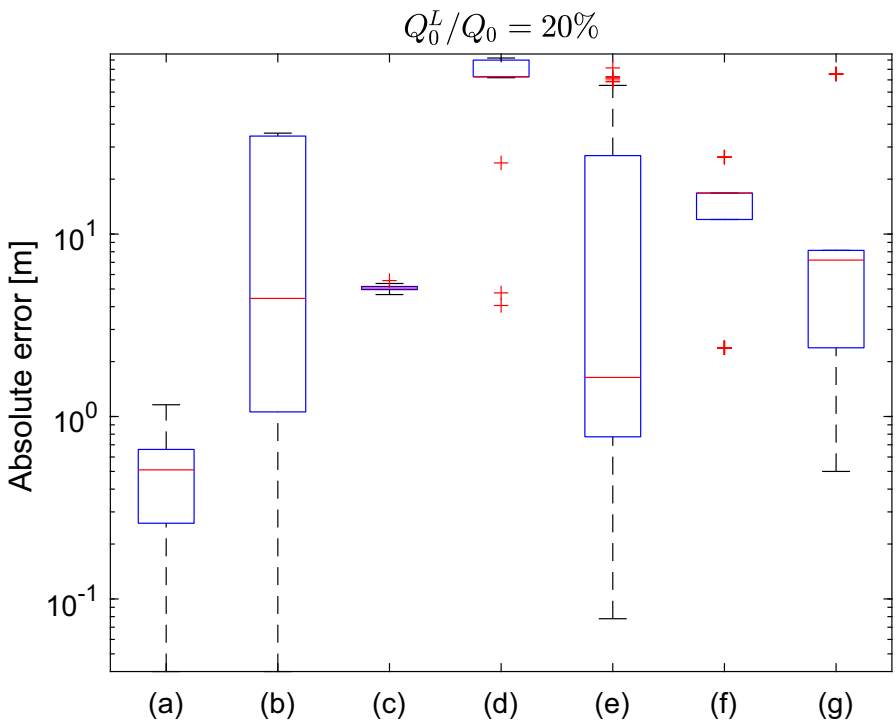

Fig. 13. Box plot of absolute error of leak localization obtained from 50 water hammer experiments. The methods used for leak localization is (a) MFP-VE with all frequencies; (b) MFP-VE with only resonant frequencies; (c) MFP-E with all frequencies; (d) MFP-E with only resonant frequencies; (e) wavelet transform method; (f) FRF peak pattern method; (g) ITA method. The ratio Q_0^L/Q_0 of leak flow and main flow is 20%.

Fig. 11(a,c,e), many peaks with almost equal height appear in the MFP objective function. However, the leak can be accurately localized by the proposed MFP with consideration of viscoelasticity (MFP-VE), where the coefficients of viscoelasticity are obtained as Section 4.1 and are displayed in Table 3, for all the three measurements (the error is 0.14 m, 0.96 m and 0.26 m, respectively). This result illustrates the robustness of the proposed method with respect to noise.

Due to the high level of noise, for each leak size ($Q_0^L/Q_0 = 40\%, 20\%, 10\%$) the experiment is repeated 50 times and the leak localization results are statistically analyzed. Here, we compare MFP-VE and MFP-E with only resonant frequencies and with more frequencies, as well as three representative methods in the literature:

- (a): MFP-VE (the method proposed in this paper) with all available frequencies $\omega \in [\omega_{th}, 17\omega_{th}]$.
- (b): MFP-VE (the method proposed in this paper) with only resonant frequencies, i.e., $\omega \in \{\omega_{th}, 3\omega_{th}, \cdots, 17\omega_{th}\}$.
- (c): MFP-E (the method in [21]) with all available frequencies $\omega \in [\omega_{th}, 17\omega_{th}]$.
- (d): MFP-E (the method in [21]) with only resonant frequencies, i.e., $\omega \in \{\omega_{th}, 3\omega_{th}, \cdots, 17\omega_{th}\}$.
- (e): The wavelet analysis method [5] (a representative of TRM) where the mother wavelet is the type Daubechies of order 1 (db1). It analyzes the drop due to leak in the first period of time signal from the hydrophone at x_1 and retains the largest drop as leak estimate.

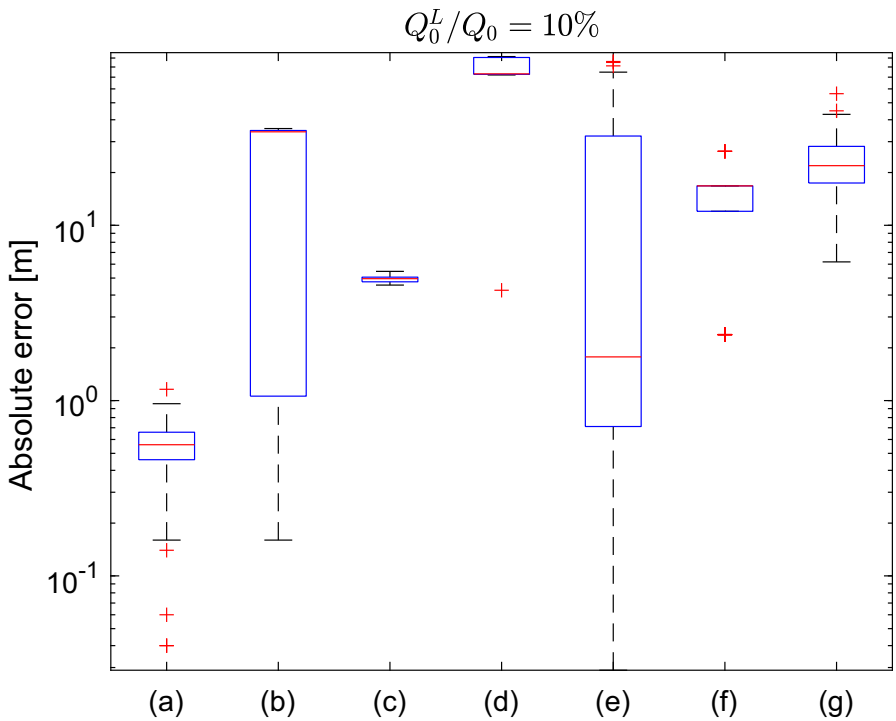

Fig. 14. Box plot of absolute error of leak localization obtained from 50 water hammer experiments. The methods used for leak localization is (a) MFP-VE with all frequencies; (b) MFP-VE with only resonant frequencies; (c) MFP-E with all frequencies; (d) MFP-E with only resonant frequencies; (e) wavelet transform method; (f) FRF peak pattern method; (g) ITA method. The ratio Q_0^L/Q_0 of leak flow and main flow is 10%.

Table 4
Statistics of absolute error of leak localization obtained from 50 water hammer experiments. The methods used for leak localization is (a) MFP-VE with all frequencies; (b) MFP-VE with only resonant frequencies; (c) MFP-E with all frequencies; (d) MFP-E with only resonant frequencies; (e) wavelet transform method; (f) FRF peak pattern method; (f) FRF peak pattern method; (g) ITA method. The ratio Q_0^L/Q_0 of leak flow and main flow is 40%.

$\lvert e \rvert$	(a)	(b)	(c)	(d)	(e)	(f)	(g)
Mean [m]	0.29	19.49	20.17	73.16	8.89	13.43	6.47
Std. [m]	0.27	16.72	26.21	24.53	17.51	8.19	3.17
Max [m]	1.24	35.54	70.14	91.54	74.95	26.42	15.26
Min [m]	0.04	0.14	4.36	4.06	0.07	2.38	0.31
5% Percentile [m]	0.04	0.14	4.76	4.36	0.21	2.38	0.5
25% Percentile [m]	0.14	0.76	5.06	72.64	0.82	2.38	4.49
50% Percentile [m]	0.16	33.19	5.26	73.09	1.74	16.78	6.95
75% Percentile [m]	0.44	34.44	24.84 m	90.64	4.77	73.16	8.14
95% Percentile [m]	0.96	35.04	69.64 m	91.24	65.18	26.42	12.02

Table 5
Statistics of absolute error of leak localization obtained from 50 water hammer experiments. The methods used for leak localization is (a) MFP-VE with all frequencies; (b) MFP-VE with only resonant frequencies; (c) MFP-E with all frequencies; (d) MFP-E with only resonant frequencies; (e) wavelet transform method; (f) FRF peak pattern method; (g) ITA method. The ratio Q_0^L/Q_0 of leak flow and main flow is 20%.

$\|e\|$	(a)	(b)	(c)	(d)	(e)	(f)	(g)
Mean [m]	0.52	17.15	5.05	74.16	17.60	14.10	12.15
Std. [m]	0.28	16.76	0.18	18.15	26.80	6.73	21.50
Max [m]	1.16	35.74	5.56	92.24	81.40	26.42	75.38
Min [m]	0.04	0.04	4.66	4.06	0.08	2.38	0.5
5% Percentile [m]	0.06	0.06	4.76	24.54	0.21	2.38	0.5
25% Percentile [m]	0.26	1.06	4.96	72.64	0.77	12.02	2.38
50% Percentile [m]	0.51	4.44	5.06	72.99	1.64	16.78	7.20
75% Percentile [m]	0.66	34.44	5.16	89.84	26.92	16.78	8.14
95% Percentile [m]	0.96	35.24	5.26	91.14	71.94	26.42	75.38

Table 6
Statistics of absolute error of leak localization obtained from 50 water hammer experiments. The methods used for leak localization is (a) MFP-VE with all frequencies; (b) MFP-VE with only resonant frequencies; (c) MFP-E with all frequencies; (d) MFP-E with only resonant frequencies; (e) wavelet transform method; (f) FRF peak pattern method; (g) ITA method. The ratio Q_0^L/Q_0 of leak flow and main flow is 10%.

$\|e\|$	(a)	(b)	(c)	(d)	(e)	(f)	(g)
Mean [m]	0.56	21.80	4.94	79.30	18.85	14.29	23.94
Std. [m]	0.24	16.51	0.21	14.08	29.14	6.74	10.61
Max [m]	1.16	35.64	5.46	91.74	85.98	26.42	56.34
Min [m]	0.04	0.16	4.56	4.26	0.03	2.38	6.18
5% Percentile [m]	0.06	0.16	4.66	72.24	0.03	2.38	9.47
25% Percentile [m]	0.46	1.06	4.76	72.64	0.71	12.02	17.43
50% Percentile [m]	0.56	34.14	4.96	73.09	1.78	16.78	21.89
75% Percentile [m]	0.56	34.74	5.06	90.64	32.31	16.78	28.20
95% Percentile [m]	0.96	35.54	5.26	91.44	81.20	26.42	42.94

Table 7
Successful rate of leak localization computed from 50 water hammer experiments in the sense of absolute error less than 1 m, 3 m, 5 m and 10 m, respectively. The methods used for leak localization is (a) MFP-VE with all frequencies; (b) MFP-VE with only resonant frequencies; (c) MFP-E with all frequencies; (d) MFP-E with only resonant frequencies; (e) wavelet transform method; (f) FRF peak pattern method; (g) ITA method.

Q_0^L/Q_0	Error	(a)	(b)	(c)	(d)	(e)	(f)	(g)
40%	⩽1 m	96%	32%	0	0	32%	0	6%
	⩽3 m	100%	44%	0	0	62%	28%	16%
	⩽5 m	100%	44%	24%	8%	76%	28%	30%
	⩽10 m	100%	44%	72%	10%	80%	28%	90%
20%	⩽1 m	96%	24%	0	0	38%	0	20%
	⩽3 m	100%	48%	0	0	60%	28%	28%
	⩽5 m	100%	50%	38%	4%	64%	20%	38%
	⩽10 m	100%	52%	100%	4%	66%	20%	90%
10%	⩽1 m	98%	22%	0	0	34%	0	0
	⩽3 m	100%	38%	0	0	58%	20%	0
	⩽5 m	100%	38%	64%	2%	64%	20%	0
	⩽10 m	100%	38%	100%	2%	68%	20%	16%

- (f): The FRF peak pattern method [14,16] (a representative of FRM; more specifically, a representative of resonant frequency based-method) which uses the peak frequencies $\omega \in \{\omega_{th}, 3\omega_{th}, \cdots, 17\omega_{th}\}$ of FRF of the hydrophone at x_1 as data for leak localization.
- (g): The inverse transient analysis (ITA) method [26] with consideration of viscoelastic effect [38]. Here, 51 potential leaks uniformly distributed in the pipe, i.e., $\{x : x = nl/50, n = 0, \cdots, 50\}$, and the sizes of the 51 potential leaks are estimated by solving a 51-parameter optimization problem. The one with highest leak size estimate is retained as leak location estimate. The measurements from all the three sensors are used. The information of actual leak location is used for the initialization of optimization (although it is not available in practice): for all the three cases of Q_0^L/Q_0, the initial leak size at the potential leak closest to the actual leak is 3.4×10^{-5} m^{-2}, while at the other potential leaks the initial sizes are all 0.

Figs. 12–14 show the box plots of absolute error of leak localization, denoted by $|e| = \left|\widehat{x^L} - x^L\right|$, in the cases of three leak sizes. Tables 4–6 display the corresponding statistics of $|e|$, including mean, standard deviation, maximum, minimum, and

Table 8
Summary of the properties of the leak localization methods.

	MFP	Wavelet	Peak pattern	ITA
Modeling viscoelasticity	Yes	No	No	Yes
Sufficient use of signal	Yes	No	No	Yes
Using multiple sensors	Yes	No	No	Yes
Initial parameter	No	No	No	Yes
Computation speed	Fast	Fast	Fast	Slow

percentiles of $|e|$. The results illustrate that MFP-VE with all frequencies is very accurate in all the three cases of leak sizes. For example, for the smallest leak where $Q_0^L/Q_0 = 10\%$ the average error is only 0.56 m, the maximum error is 1.16 m, and in 49 over 50 tests the leak localization error is less than 1 m. The average error is lower for the larger leaks. Both considering viscoelasticity and using more frequencies are essential for the accuracy of MFP leak localization: the methods (b), (c) and (d) all have much higher error than (a). The methods (e), (f) and (g) also have relatively large error of leak localization. It is remarkable that for the FRF peak pattern method (f), due to only nine FRF peaks are available, the resolution of leak localization is actually very low that leak location estimate can only be chosen from nine candidates along the pipe. Similarly, the resolution of ITA method (g) is decided by the distribution of potential leaks; here, the resolution of (g) is $l/100 = 1.44$ m because the leak is selected from $\{x : x = nl/50, n = 0, \cdots, 50\}$ (51 potential leaks are assumed in this case).

In practice, excavation cost is proportional to range of possible leak location, therefore leak localization with accuracy less than a threshold is of importance. Successful rate of leak localization in the sense of absolute error $|e|$ less than 1 m, 3 m, 5 m and 10 m, computed from the 50 transient experiments, is shown in Table 7. Again, MFP-VE with all frequencies (a) outperforms other methods. The wavelet method (e), which does not need many pipe parameters such as viscoelasticity coefficients, has error less than 5 m in most cases which is also acceptable in this sense.

5. Discussions

In this section, the experimental results and the leak localization methods are more profoundly discussed, in the following aspects.

- *Modeling physical complexity*: An advantage of the MFP approach proposed in this paper is that this method considers the viscoelasticity effect of pipe wall, which largely modifies the behavior of transient wave in pipe and measured data. The physical model-dependent methods such as MFP can produce very accurate leak localization. However, its accuracy depends on the correctness of the physical model. When the elastic (wrong) model is used in the viscoelastic case, i.e., the methods (c) and (d), or the viscoelastic coefficients cannot be satisfactorily given, the localization is not accurate. In the case that accurate model is not available, methods less dependent on physical model, such as the wavelet method (e), is an option.
- *Sufficient use of information from measurements*: It has been shown in the literature that many leak detection methods using partial information (reflection, damping, resonant frequencies, etc.) work well in ideal environments. However, in real experiments which are usually very noisy, the used partial information is very possibly contaminated such that these methods fail. A solution is to use as much information as possible. This paper experimentally justifies this issue: the method (a), which uses all available information, outperforms the method (b), which uses only resonant frequencies, and the method (e), which uses only the reflection due to leak in the first period. This issue has also been justified numerically in [21] and theoretically via the theory of Fisher information and Cramér-Rao lower bound (CRLB) [22,54]: each time step of the time signal or each frequency in the FRF are useful information for leak detection and decreases the expected estimation error.
- *Multi-sensor fusion*: Again, due to the presence of noise, it is preferable to use as much information as possible. Except using more frequencies and time signals, another approach is to set more sensors in the pipe. MFP (as well as ITA) is able to fuse information from different sensors, without changing the algorithm but only increases the length of the vectors $\Delta\mathbf{h}$ and $\mathbf{G}$ in Eq. (36).
- *Computation complexity*: MFP and ITA has the similarity that both methods decide the leak by matching the measured data with the physical model. However, ITA needs to solve a multiple-parameter optimization problem; its dimension equals to the number of potential leaks assumed in the pipe. Therefore, a high localization resolution or precision of ITA implies an extremely slow computation and vice versa. Also, the result of ITA strongly depends on the initial value and it is very possible that the algorithm stops at local maximum which corresponds to a bad result. By contrast, the matching of MFP only needs to solve a 1D optimization, therefore a 1D search/plot of MFP objective function versus leak location along the pipe is sufficient. This implies that MFP has a fast computation, does not need initial guess of leak, and avoids local maximum traps.

The above discussion regarding the properties of the leak localization methods is briefly summarized in Table 8.

6. Conclusion

This paper addresses the problem of leakage localization in a viscoelastic pipe. The viscoelasticity of pipe wall is modeled in the governing equations of transient wave and, in the frequency domain, the viscoelastic effect is equivalent to modifying the transfer matrix with a frequency-dependent wave speed. Then, matched-field processing (MFP), which has been proposed for leakage detection in elastic pipes, is generalized for the viscoelastic case.

Transient experiment results with viscoelastic pipe in the Water Engineering Laboratory at University of Perugia and in the Water Resources Research Laboratory at Hong Kong University of Science and Technology are both studied to assess the proposed method. It is shown that both considering pipe wall viscoelasticity and using more frequencies (instead of using only the resonant frequencies) in the leakage localization scheme are essential for leak localization accuracy. The proposed MFP method outperforms classical leakage detection methods in the literature in the sense of lower leak localization error. For a small leak where the flow ratio of leak and main pipe is 10%, MFP is very accurate that, in 49 of 50 experiments, the leak localization error is lower than 1 m (the error of the rest one is 1.14 m), although some of these signals are seriously contaminated by noise.

Further work may be conducted in several directions. First, the generalization of the results to more complicated cases, for example localization of multiple leaks and application to more complex piping systems, would be important. Besides, this paper uses the pipe wall viscoelastic coefficients obtained from a no-leak test, which may not be available in some practical cases. Therefore, a method that can jointly estimate leaks and the viscoelastic coefficients would be desirable.

Acknowledgements

This work has been supported by research grants from the Research Grant Council of Hong Kong SAR (Project No.: T21-602/15R), Chinese Estates Professorship in Engineering (No.: R8031), and Italian MIUR and University of Perugia within the program Dipartimenti di Eccellenza 2018–2022. The authors would like to thank Duncan A. McInnis, Asgar Ahadpour Dodaran, Man Yue Lam, Moez Louati, Muhammad Waqar, and Kamrun Nahar Keya for their helps on the experiments at Hong Kong University of Science and Technology.

References

[1] A.F. Colombo, P. Lee, B.W. Karney, A selective literature review of transient-based leak detection methods, J. Hydro-Environ. Res. 2 (4) (2009) 212–227.
[2] B. Brunone, Transient test-based technique for leak detection in outfall pipes, J. Water Resour. Planning Manage. 125 (5) (1999) 302–306.
[3] B. Brunone, M. Ferrante, Detecting leaks in pressurised pipes by means of transients, J. Hydraul. Res. 39 (5) (2001) 539–547.
[4] D. Covas, H. Ramos, N. Graham, C. Maksimovic, Application of hydraulic transients for leak detection in water supply systems, Water Sci. Technol.: Water Supply 4 (5–6) (2005) 365–374.
[5] M. Ferrante, B. Brunone, S. Meniconi, Wavelets for the analysis of transient pressure signals for leak detection, J. Hydraul. Eng. 133 (11) (2007) 1274–1282.
[6] S. Meniconi, B. Brunone, M. Ferrante, C. Capponi, C.A. Carrettini, C. Chiesa, D. Segalini, E.A. Lanfranchi, Anomaly pre-localization in distribution–transmission mains by pump trip: preliminary field tests in the milan pipe system, J. Hydroinf. 17 (3) (2015) 377–389.
[7] S.T.N. Nguyen, J. Gong, M.F. Lambert, A.C. Zecchin, A.R. Simpson, Least squares deconvolution for leak detection with a pseudo random binary sequence excitation, Mech. Syst. Signal Process. 99 (2018) 846–858.
[8] X.-J. Wang, M.F. Lambert, A.R. Simpson, J.A. Liggett, J.P. Vítkovský, Leak detection in pipelines using the damping of fluid transients, J. Hydraul. Eng. 128 (7) (2002) 697–711.
[9] J.C.P. Liou, Pipeline leak detection by impulse response extraction, J. Fluids Eng. 120 (4) (1998) 833–838.
[10] W. Mpesha, S.L. Gassman, M.H. Chaudhry, Leak detection in pipes by frequency response method, J. Hydraul. Eng. 127 (2) (2001) 134–147.
[11] M. Ferrante, B. Brunone, Pipe system diagnosis and leak detection by unsteady-state tests. 1. Harmonic analysis, Adv. Water Resour. 26 (1) (2003) 95–105.
[12] D. Covas, H. Ramos, A.B. De Almeida, Standing wave difference method for leak detection in pipeline systems, J. Hydraul. Eng. 131 (12) (2005) 1106–1116.
[13] P.J. Lee, J.P. Vitkovsky, M.F. Lambert, A.R. Simpson, and J.A. Liggett. Frequency response coding for the location of leaks in single pipeline systems. The Int. Conference on Pumps, Electromechanical Devices and Systems Applied to Urban Water Management, IAHR and IHRA, Valencia, Spain, April 22–25, 2003.
[14] P.J. Lee, J.P. Vítkovský, M.F. Lambert, A.R. Simpson, J.A. Liggett, Leak location using the pattern of the frequency response diagram in pipelines: a numerical study, J. Sound Vib. 284 (3) (2005) 1051–1073.
[15] P.J. Lee, J.P. Vítkovský, M.F. Lambert, A.R. Simpson, J.A. Liggett, Frequency domain analysis for detecting pipeline leaks, J. Hydraul. Eng. 131 (7) (2005) 596–604.
[16] P.J. Lee, M.F. Lambert, A.R. Simpson, J.P. Vítkovský, J. Liggett, Experimental verification of the frequency response method for pipeline leak detection, J. Hydraul. Res. 44 (5) (2006) 693–707.
[17] A.M. Sattar, M.H. Chaudhry, Leak detection in pipelines by frequency response method, J. Hydraul. Res. 46 (EI1) (2008) 138–151.
[18] M. Taghvaei, S.B.M. Beck, J.B. Boxall, Leak detection in pipes using induced water hammer pulses and cepstrum analysis, Int. J. Comadem 13 (1) (2010) 19.
[19] H.-F. Duan, P.J. Lee, M.S. Ghidaoui, Y.-K. Tung, Leak detection in complex series pipelines by using the system frequency response method, J. Hydraul. Res. 49 (2) (2011) 213–221.
[20] I. Rubio Scola, G. Besançon, D. Georges, Blockage and leak detection and location in pipelines using frequency response optimization, J. Hydraul. Eng. 143 (1) (2016) 04016074.
[21] X. Wang, M.S. Ghidaoui, Pipeline leak detection using the matched-field processing method, J. Hydraul. Eng. 144 (6) (2018) 04018030.
[22] X. Wang, M.S. Ghidaoui, Identification of multiple leaks in pipeline: Linearized model, maximum likelihood, and super-resolution localization, Mech. Syst. Signal Process. 107 (2018) 529–548.
[23] X. Wang, D.P. Palomar, L. Zhao, M.S. Ghidaoui, R.D. Murch, Spectral-based methods for pipeline leakage localization, J. Hydraul. Eng. 145 (3) (2019) 04018089, https://doi.org/10.1061/(ASCE)HY.1943-7900.0001572.

[24] X. Wang, M.S. Ghidaoui, Identification of multiple leaks in pipeline II: Iterative beamforming and leak number estimation, Mech. Syst. Signal Process. 119 (2019) 346–362.
[25] B. Zhou, A. Liu, X. Wang, Y. She, V. Lau, Compressive sensing-based multiple-leak identification for smart water supply systems, IEEE Internet Things J. 5 (2) (2018) 1228–1241.
[26] J.A. Liggett, L.-C. Chen, Inverse transient analysis in pipe networks, J. Hydraul. Eng. 120 (8) (1994) 934–955.
[27] J.P. Vítkovský, A.R. Simpson, M.F. Lambert, Leak detection and calibration using transients and genetic algorithms, J. Water Resour. Planning Manage. 126 (4) (2000) 262–265.
[28] M.L. Stephens, Transient Response Analysis for Fault Detection and Pipeline Wall Condition Assessment in Field Water Transmission and Distribution Pipelines and Networks, University of Adelaide, 2008 (Ph.D. thesis).
[29] D. Covas, H. Ramos, Case studies of leak detection and location in water pipe systems by inverse transient analysis, J. Water Resour. Planning Manage. 136 (2) (2010) 248–257.
[30] P.G. Franke, Computation of unsteady pipe flow with respect to visco-elastic material properties, J. Hydraul. Res. 21 (5) (1983) 345–353.
[31] G. Pezzinga, P. Scandura, Unsteady flow in installations with polymeric additional pipe, J. Hydraul. Eng. 121 (11) (1995) 802–811.
[32] D. Covas, I. Stoianov, H. Ramos, N. Graham, C. Maksimovic, The dynamic effect of pipe-wall viscoelasticity in hydraulic transients. Part i-experimental analysis and creep characterization, J. Hydraul. Res. 42 (5) (2004) 517–532.
[33] D. Covas, I. Stoianov, J.F. Mano, H. Ramos, N. Graham, C. Maksimovic, The dynamic effect of pipe-wall viscoelasticity in hydraulic transients. Part ii-model development, calibration and verification, J. Hydraul. Res. 43 (1) (2005) 56–70.
[34] A. Keramat, A.S. Tijsseling, Q. Hou, A. Ahmadi, Fluid-structure interaction with pipe-wall viscoelasticity during water hammer, J. Fluids Struct. 28 (2012) 434–455.
[35] H.-F. Duan, M. Ghidaoui, P.J. Lee, Y.-K. Tung, Unsteady friction and visco-elasticity in pipe fluid transients, J. Hydraul. Res. 48 (3) (2010) 354–362.
[36] H.-F. Duan, P.J. Lee, M.S. Ghidaoui, Y.-K. Tung, System response function-based leak detection in viscoelastic pipelines, J. Hydraul. Eng. 138 (2) (2011) 143–153.
[37] S. Meniconi, B. Brunone, M. Ferrante, C. Massari, Numerical and experimental investigation of leaks in viscoelastic pressurized pipe flow, Drinking Water Eng. Sci. 6 (1) (2013) 11.
[38] A.K. Soares, D.I.C. Covas, R.R. Luisa Fernanda, Leak detection by inverse transient analysis in an experimental PVC pipe system, J. Hydroinf. 13 (2) (2011) 153–166.
[39] M.T. Shaw, W.J. MacKnight, Introduction to Polymer Viscoelasticity, John Wiley & Sons, 2005.
[40] P.J. Lee, J.P. Vítkovský, Quantifying linearization error when modeling fluid pipeline transients using the frequency response method, J. Hydraul. Eng. 136 (10) (2010) 831–836.
[41] M.H. Chaudhry, Applied Hydraulic Transients, third ed., Springer, 2014.
[42] E.B. Wylie, V.L. Streeter, L. Suo, Fluid transients in systems, vol. 1, Prentice Hall Englewood Cliffs, NJ, 1993.
[43] A. Kashima, P.J. Lee, R. Nokes, Numerical errors in discharge measurements using the KDP method, J. Hydraul. Res. 50 (1) (2012) 98–104.
[44] A. Kashima, P.J. Lee, M.S. Ghidaoui, M. Davidson, Experimental verification of the kinetic differential pressure method for flow measurements, J. Hydraul. Res. 51 (6) (2013) 634–644.
[45] A. Dubey, Z. Li, P.J. Lee, R. Murch, Observations of acoustic noise in water supply pipeline systems, J. Acoust. Soc. Am. (2019), Under Review.
[46] J. Lin, X. Wang, M.S. Ghidaoui, Theoretical investigation of leak's impact on normal modes of a water-filled pipe: from small to large leak impedance, J. Hydraul. Eng. (2019), https://doi.org/10.1061/(ASCE)HY.1943-7900.0001606.
[47] B. Brunone, A. Berni, Wall shear stress in transient turbulent pipe flow by local velocity measurement, J. Hydraul. Eng. 136 (10) (2010) 716–726.
[48] P.J. Lee, Using System Response Functions of Liquid Pipelines for Leak and Blockage Detection, The University of Adelaide, Adelaide AU, 2005 (Ph.D. thesis).
[49] P.A. Lynn, An introduction to the analysis and processing of signals, McMillan (1973).
[50] G. Pezzinga, B. Brunone, S. Meniconi, Relevance of pipe period on Kelvin-Voigt viscoelastic parameters: 1D and 2D inverse transient analysis, J. Hydraul. Eng. 142 (12) (2016) 04016063.
[51] B. Brunone, S. Meniconi, C. Capponi, Numerical analysis of the transient pressure damping in a single polymeric pipe with a leak, Urban Water J. 15 (8) (2018) 760–768.
[52] S. Meniconi, B. Brunone, M. Ferrante, C. Massari, Energy dissipation and pressure decay during transients in viscoelastic pipes with an in-line valve, J. Fluids Struct. 45 (2014) 235–249.
[53] M. Ferrante, B. Brunone, S. Meniconi, B.W. Karney, C. Massari, Leak size, detectability and test conditions in pressurized pipe systems, Water Resour. Manage 28 (13) (2014) 4583–4598.
[54] A. Keramat, M.S. Ghidaoui, X. Wang, M. Louati, Cramer-Rao lower bound for performance analysis of leak detection, J. Hydraul. Eng. (2019), https://doi.org/10.1061/(ASCE)HY.1943-7900.0001603.